Institute for Sustainable Energy, University of Malta

SUSTAINABLE ENERGY 2016:
THE ISE ANNUAL CONFERENCE

Tuesday 4th October 2016, The Auditorium, University of Malta, Valletta Campus, Malta

ISBN 978-99957-853-1-4

ANALYSIS OF A NOVEL OFFSHORE PLATFORM WITH INTEGRATED ENERGY STORAGE OPERATING IN CENTRAL MEDITERRANEAN WATERS

D. Buhagiar[1], T. Sant[1] and R.N. Farrugia[2]
[1]Department of Mechanical Engineering, University of Malta, Msida MSD 2080, Malta
[2]Institute for Sustainable Energy, University of Malta, Triq il-Barrakki, Marsaxlokk MXK 1531, Malta
Corresponding Author E-mail: daniel.buhagiar@um.edu.mt

ABSTRACT: A thermodynamic model of a novel energy storage device is described and simulated in the context of a central Mediterranean climate. The device uses a hydro-pneumatic concept to store energy as compressed air. It is designed to be integrated into an offshore floating platform. The thermodynamic model illustrates the behaviour of the compression process and the heat exchange with the surrounding environment. Different rates of compression are simulated, and it can be observed that faster compression rates lead to higher gas temperatures and pressures. The sensitivity to climatic conditions is also investigated, however this effect was seen to be minimal. A simplified Black-Box Model is also developed, with its parameters obtained through a curve-fitting process. Finally, a stochastic input is fed to both models and a comparison is made. The simplified model results in a minor over-prediction of the efficiency.

Keywords: Offshore Renewable Energy, Compressed Air Storage, Isobaric Accumulator

1 INTRODUCTION

The widespread integration of renewable energy systems will rely on technologies that can continuously meet varying demands using an intermittent supply. Studies indicate that significant back up will be required even if renewables can cover 100% of the demand [1].

Energy storage comprises promising technologies that can mitigate the mismatch between supply and demand [2]. Some of the specific applications include frequency control, load balancing and peak shaving. The decarbonisation of energy production will result in increased deployment of energy storage [3].

Generation Integrated Energy Storage (GIES) [4] is a relatively new approach to energy storage and renewables. The aim is to store energy in its primary form and thus reduce inefficiencies. Research at the University of Malta has focussed on wind energy generation, specifically on offshore wind energy. The advantages of the offshore environment in this context are extensively documented [4]. Moreover, co-locating an energy storage device in the offshore environment can also be highly beneficial [5].

On-going work has shown the advantages of using hydraulic power transmission instead of electrical transmission in large-scale offshore wind farms [6] [7]. This would result in replacing the gearbox and generator inside the nacelle with a positive displacement pump. The pump is directly connected to the rotor and transmits pressurised fluid across the network. The combined farm output can be converted into electricity at a centralised, possibly onshore, hydroelectric station.

The integration of a hydraulic energy storage device would provide a suitable form of GIES. However, conventional hydraulic accumulators are not suitable for storing large quantities of energy. They are typically suited to mitigating very short fluctuations in relatively smaller circuits. The main challenge is that conventional designs would experience very significant pressure fluctuations as they charge and discharge. This hinders their integration into hydraulic power transmission circuits that would require a fixed, stable pressure.

A device currently under development at the University of Malta is attempting to address this issue by using a liquid-piston [8] and an additional compressed air chamber. This compressed air chamber is integrated into a floating platform to provide stabilising upthrust and a means of mitigating pressure fluctuations. This symbiotic design combines the *power density* of hydraulics and the *energy density* of pneumatics.

This paper pertains to an analytical model of the device, with a focus on the gas thermodynamics. The model is fed with an intermittent energy input and its performance under different conditions in a central Mediterranean climate is monitored.

2 ANALYTICAL MODEL

2.1 Design Principles

The storage system is designed to mitigate pressure fluctuations using an external compressed air chamber. This principle is best described using a pressure-volume diagram as shown in Figure 1. The operational volume is retained in the liquid-piston portion, with the rest of the volume only serving to mitigate the pressure fluctuations. The two chambers are connected by an umbilical pipeline.

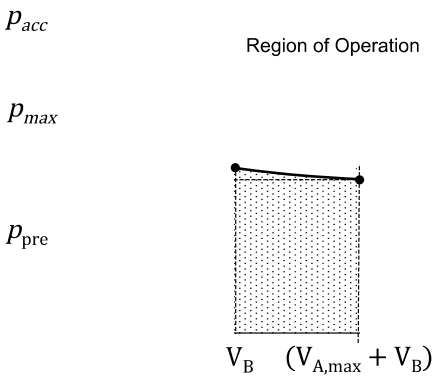

Figure 1: *p-V* diagram **showing the physical behaviour of the gas in such a device**

The external portion does not only serve to mitigate pressure changes, but also provides stabilising upthrust to the platform. This makes it more feasible from a technical perspective and the hollow floating portion could potentially assist in the installation of the system. The integration of this design into a floating Tension Leg Platform (TLP) is shown in Figure 2. Key design attributes were maintained; these include the *gross displacement*, *overall mass* and *centre of gravity* position relative to the centre of buoyancy.

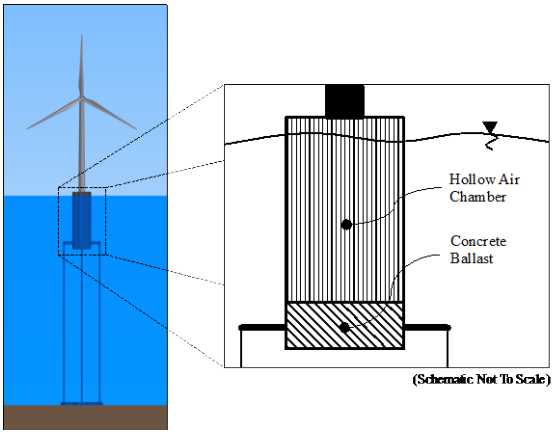

Figure 2: NREL/MIT-TLP **[10]** to scale at 200 m depth with the proposed liquid piston accumulator (also to scale) on the seabed and a cross-section of the floating platform (not to scale).

The baseline design under investigation is based on a well-understood TLP designed for offshore wind turbines. Referred to as the NREL/MIT-TLP [10], it was planned for a 5MW turbine. When integrated into such a platform, the FLASC concept would result in around 5.2MWhr of integrated energy storage capacity.

2.2 Thermodynamic Model

The model is described in detail in existing work [11]. In the present context, an overview of the fundamental equations is presented.

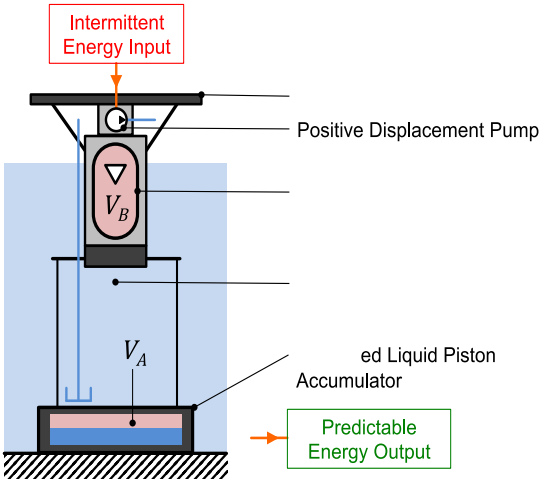

Figure 3**:** Simplified Schematic of the Device (reproduced from [11]).

The system can be described as two interconnected air chambers having a variable (V_A) and fixed (V_B) volume (Figure **3**); the former being the chamber comprising the liquid piston. The continuity equation for this component is as follows:

$$\dot{m}_A = \frac{A_A}{RT_A} p_A \frac{dx_i}{dt} - \frac{V_{init} - x_i A_A}{RT_A}\left[\frac{dp_A}{dt} - \frac{p_A}{T_A}\frac{dT_A}{dt}\right] \quad (1)$$

$$V_A = V_{init} - x_i A_A \quad (2)$$

In the above equations x_i and A_A are the position and area of the liquid-piston interface respectively. V_{init} is the initial air volume and $\dot{m}_A$ is the mass flow rate out of the chamber.

Applying the energy equation gives the rate of change in internal energy:

$$q_A = \frac{p_A c_p A_A}{R}\left(\frac{dx_i}{dt}\right) - \frac{c_v}{R}(V_{init} - x_i A_A)\frac{dp_A}{dt} - q_{w,A} \quad (3)$$

where c_p, c_v are the specific heat capacities of the air and $q_{w,A}$ is the heat lost through the walls.

A similar set of equations can also be obtained for the fixed volume chamber:

$$\dot{m}_B = \frac{V_B}{RT_B}\left[\frac{dp_B}{dt} - \frac{p_B}{T_B}\frac{dT_B}{dt}\right] \quad (4)$$

$$q_B = \frac{c_v V_B}{R}\frac{dp_B}{dt} + q_{w,B} \quad (5)$$

An additional equation relates the pressures in the two portions (p_A, p_B) by quantifying the drop across the umbilical conduit [11]. Turbulent frictional losses are calculated using a friction factor. It must be noted that frictional heating and the compressibility of the air in the umbilical connector are neglected. Both of these phenomena tend to be negligible in this context. Finally, the heat flux through the umbilical connection can be quantified as follows:

$$q_A = c_p T_A \dot{m}_{umb} \quad (4)$$

The above equation set is solved using a first-order Euler method programmed in MATLAB™.

2.3 Boundary Conditions

The above equation set allows simulation of the response for known boundary conditions. Such conditions are required to quantify the heat exchanged with the surroundings during the charging or discharging process.

Heat exchange processes occur primarily across the solid cross-section of the structure and also across the liquid-gas interface of the liquid piston. For the cases of conduction across a solid interface, a lumped model is adopted to account for the thermal inertia of the cross-section. It treats each element of the cross-section as a thermal mass, with a resistive term on each side. The resistive term represents the resistance to heat transfer of half the cross-sectional thickness. A thermal network representation (Figure 4) is then undertaken to combine the various elements.

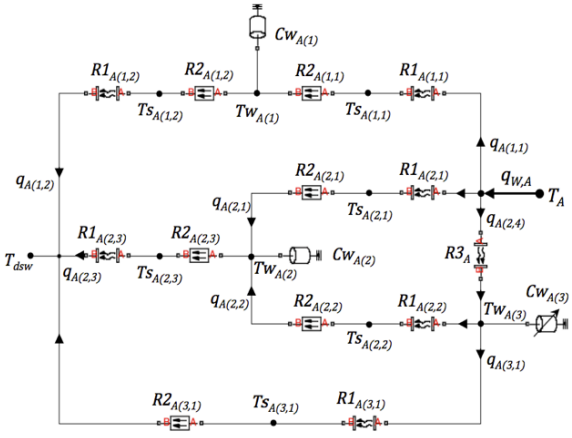

Figure 4: Thermal Network: Bottom Chamber

The network elements $R1_{A(i,j)}$ represent the resistance to heat transfer between the fluid and solid surfaces. Elements $R2_{(i,j)}$ represent conduction resistance through the solid wall, where $Tw_{A(i)}$ and $Cw_{A(i)}$ represent the temperature and heat capacity of that wall. Finally, the term $R3_A$ represents the resistance to heat transfer across the liquid-gas interface and $Cw_{A(3)}$ is the heat capacity of the mass of stored seawater, which changes throughout the simulation. Terms $q_{A(i,j)}$ represent the heat fluxes. Heat transfer coefficients are quantified using the relevant empirical correlations based on the Rayleigh and Nusselt numbers.

Resistance to heat transfer across the liquid-gas interface is computed using the equation of Kermani and Rokni [12]:

$$R_{l/g} = \frac{1}{A_A}\left(\frac{L_{gas}}{k_{gas}} + \frac{L_{liq}}{k_{liq}}\right) \quad (5)$$

where k_{gas} and k_{liq} are the thermal conductivities of the gas and liquid portions and L_{gas} and L_{liq} are their axial thicknesses.

During storage, cold liquid is pumped into the chamber and this affects the internal energy within the system. A simple isobaric mixing process between the fluid being pumped in and the fluid already within the chamber is therefore considered to account for this effect.

The system is intended for deployment in the offshore environment at depths of around 200 m. The temperatures of the surrounding water are obtained from monthly data of the US National Oceanic and Atmospheric Administration [13].

Data for the central Mediterranean island of Malta is shown in Figure **5**. Here the formation of a thermocline layer can be observed for the warmer months. This implies that the air in the floating chamber (V_B) is surrounded by much warmer temperatures when compared to the air in the chamber on the seabed (V_A). The analytical model will allow observation of any differences in the way the two chambers behave.

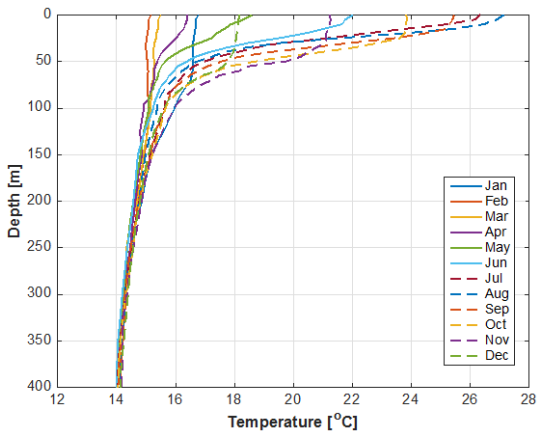

Figure 5: Temperature-Depth profiles for Maltese coastal waters [13]

3 SIMPLIFIED BLACK-BOX MODEL

The model developed in [11] and briefly described above is highly accurate when it comes to resolving the thermodynamic processes involved. However, this comes with significant computational demands. A Black-Box Model was also developed in order to allow simulation of the storage device operating in the context of a larger system, or when being fed with long stochastic data sets. It uses a simple polytropic compression law for an ideal gas. The ideal gas assumption is also applied to the analytical model, justified by compressibility factors that are close to unity for all relevant conditions [11]. The simplified model can be expressed as follows:

$$p_{acc}(t) = p_{pre}\left(\frac{V_{tot}}{V_A(t) + V_B}\right)^n \quad (6)$$

The instantaneous accumulator pressure (p_{acc}) can therefore be obtained as a function of the instantaneous volume of air in the lower chamber (V_A), obtained from equation (2). Terms p_{pre} and V_{tot} are the pre-charge pressure and total air volume respectively, while n is the polytropic index.

Obtaining a suitable polytropic index is the scope of the present work. This is calculated by using a curve-fitting algorithm on data obtained from the detailed analytical model. The sensitivity of this fixed polytropic index to different compression rates is also analysed.

For the system operating with an intermittent flow input and fixed output flow requirement, the instantaneous volume of air in the lower chamber (V_A) can be obtained as follows:

$$V_A^{(i)} = V_A^{(i-1)} + Q_{acc}\Delta t \quad (7)$$

where $V_A^{(i-1)}$ is the volume at the previous time step and Δt is the length of that time-step. The flow into the accumulator is given by the difference between the input (available) flow (Q_{in}) and the fixed flow demand (Q_{dem}):

$$Q_{acc} = Q_{in} - Q_{dem} \quad (8)$$

As the accumulator charges and discharges, its pressure will also change. In practice a nozzle controller will be in place to ensure that the flow demand is being delivered, despite minor changes in pressure. Given the advantageous design of the accumulator, this can be easily achieved using a variable area orifice. The flow demand is based on the mean energetic content of the 24 hour wind data. The input flow is obtained from artificial wind data and a transient model of a hydraulic wind turbine developed in previous work [14].

One major drawback of this simplified approach is its inability to account for heat exchange when the system is not being charged or discharged. However, the implication of this shortcoming is quantified in cases when the system is fed stochastic flow data and must provide a fixed, steady output. Once again, a comparison to the detailed model is made in order to observe any deficiencies in the Black-Box Model.

4 SIMULATION RESULTS

Simulations are carried out for the baseline system having the default parameters shown in Table 1. In all cases, the internal air temperature starts in equilibrium with the surroundings.

The first set of results focuses on the use of the analytical model. A number of charging cycles are simulated with the scope of obtaining a mean polytropic index for the system. This is followed by a comparison between the computational cost of this detailed model and the simplified Black-Box Model. The criteria are the discrepancy in the predicted pressure response and overall efficiency in a simulation using stochastic wind data.

Table 1: Storage System Parameters

Umbilical Diameter / Length	0.2 m / 146.2 m
Chamber A Volume	1,300 m^3
Chamber B Volume	12,200 m^3
Chamber A Material	Concrete, Dense
Chamber B Material	Steel, Carbon 1%
Umbilical Conduit Material	GRE/GRP
Pre-Charge Pressure	150 bar
Seawater Initial Temperature	14.7˚C
System Operating Depth	200 m

4.1 Effect of Compression Rate

The parameter under investigation is the charging rate. This primarily affects the time available for the internal gas to dissipate heat as it is being compressed. It also affects the ability of the umbilical connector to transfer air from the bottom to the upper chamber, and hence the pressure distribution in the system. A range of charging rates is simulated based on the typical output from a 5MW hydraulic turbine [7] as shown in Table 2.

Table 2: Simulated Charging Rates

Turbine Condition	Wind Speed [ms^{-1}]	Charging Rate [m^3s^{-1}]
Intermediate 1	5	0.024
Intermediate 2	7	0.073
Intermediate 3	9	0.158
Rated	11.4	0.310

Table 3: Max. Values at Different Charging Rates

Charging Rate [m^3s^{-1}]	p_A [bar]	p_B [bar]	T_A [˚C]	T_B [˚C]
0.024	169.6	169.4	28.5	29.0
0.073	172.1	172.3	33.5	34.3
0.158	174.3	174.0	36.6	37.3
0.310	175.8	175.0	38.4	39.0

The resulting maximum pressures and temperatures are shown in Table 3. It can be observed that the faster the charging rate, the higher the temperature (and pressure). This is because during a fast compression process the air does not have time to dissipate heat. In all cases the pressure is well distributed between the two chambers.

A pressure-cycle was simulated for the two months experiencing the extreme temperatures: i.e. February and September. The energy is held for a period of 24 hours and then discharged. The system is then allowed to stabilise for a further 24 hours. An intermediate charging/discharging rate of 0.158 m^3s^{-1} was used in both cases. The pressure and temperature responses of the system are shown in Figure 6 and Figure 7 respectively.

Here one can observe a sharp increase in pressure as the system charges. This is primarily due to the compression stroke itself, but there is also some compression heating. In fact, as the charging stops at the 2-hour mark, the gas begins to cool down and an associated drop is observed. This temperature change can also be observed in Figure 7. Conversely, during the discharging process the gas cools down and re-absorbs some heat from the surroundings as the system stabilises.

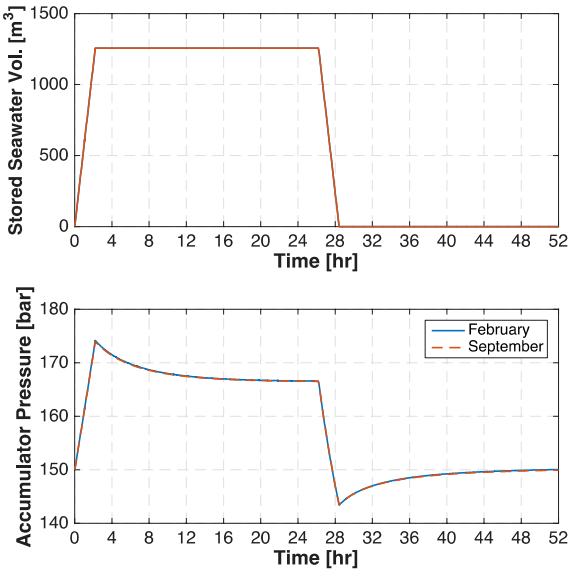

Figure 6: Charge/discharge cycles for February and September: Pressure Response.

The p-V diagram in Figure **8** confirms that the response and efficiencies are practically identical for the two extreme months of February (95.18%) and September (95.22%). This implies that consistent performance across different climatic conditions can be achieved.

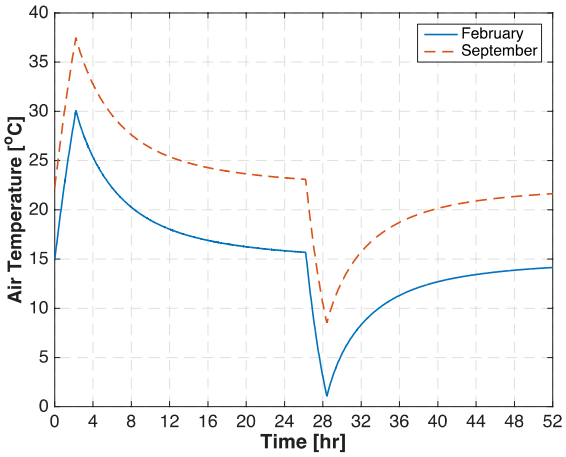

Figure 7: Charge/discharge cycles for February and September: Temperature Response.

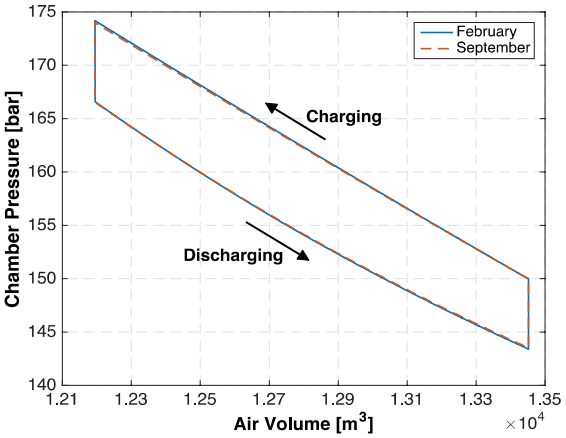

Figure 8: Pressure-volume diagrams for February and September.

4.2 Establishing a Mean Polytropic Index

The principal objective of this work is to obtain a fixed polytropic index that describes the thermodynamic process. In order to obtain this value a curve-fitting procedure was used on the pressure response for different compression rates. Based on well-established physical principles, a pre-defined form was used, leaving only a single unknown variable. From equation (6):

$$p(V) = p_{pre}\left(\frac{V_{tot}}{V}\right)^n \tag{9}$$

Data for (p, V) resulting from the analytical model was fitted to the above form and the values obtained for the polytropic index are tabulated below. The term (p_{err}) describes the error, relative to the pre-charge pressure, between the final pressure predicted by the analytical model and the fixed polytropic index.

Table 4: Polytropic Index Regression Analysis

Charging Rate [m^3s^{-1}]	n [-]	R^2 [-]	p_{err} [-]
0.024	1.304	0.9892	-0.65%
0.073	1.467	0.9957	-0.68%
0.158	1.546	0.9987	-0.31%
0.310	1.587	0.9997	+0.15%

It can be observed that there is a very strong correlation throughout. The best fit is for the highest compression rate, shown in Figure 9. Also shown is the lowest compression rate, which had the poorest fit. The higher rate corresponds to an almost adiabatic scenario where the air has very limited time to dissipate heat as it is being compressed. It can also be noted that the polytropic index is above 1.4. At higher pressures, the specific heat at constant pressure increases more drastically than the specific heat at constant volume, resulting in an increase in their ratio (γ). The analytical model accounts for this, and rightfully yields such higher values. Interpolating from thermodynamic properties of air [15] results in a value: $\gamma = 1.63$ at the prescribed conditions.

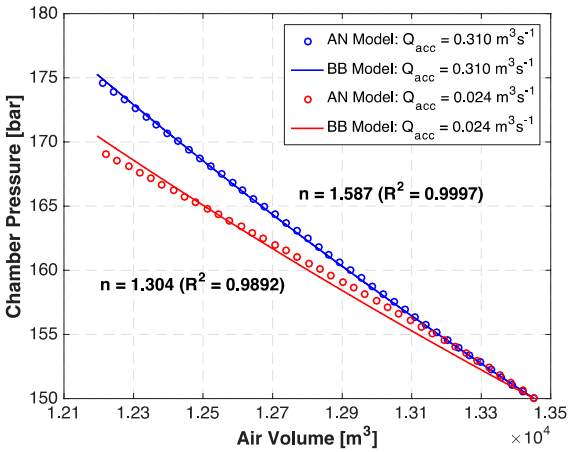

Figure 9: Polytropic Index Regression Analysis

4.3 Comparison of the Two Models

There is quite a range of polytropic indices, as shown in Table 4. In order to best select a value suitable for real-time stochastic simulations, a full 24-hour run was carried out using wind data. A comparison is then drawn between the resulting pressure response from the analytical model and the response predicted by the Black-Box Model using fixed polytropic indices. This comparison is quantified using an Accumulated Error (AE) function:

$$\mathrm{AE} = \frac{1}{n_s}\left\{\sum_{i=1}^{n_s}(p_{an}[t_s] - p_{bb}[t_s])^2\right\}^{\frac{1}{2}} \qquad (10)$$

where n_s is the number of samples, p_{an} and p_{bb} represent the pressures predicted by the analytical and Black Box Models at a sample time t_s.

The analytical model was run using 24 hours of wind data having a mean wind speed of 7.0 ms^{-1} and a turbulence intensity of 10% with the storage device initially half full. The model was programmed to store and dissipate energy in order to provide a fixed power output corresponding to the mean energetic content of the 24 hour time-series. The conversion of free stream kinetic energy into hydraulic power is outside the scope of this work but is documented in [14].

The Black-Box Model was programmed in a similar manner. In this case, a number of runs were carried out using a variety of polytropic indices. The AE was calculated for each value.

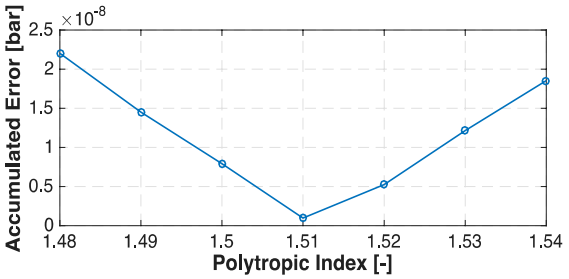

Figure 10: Accumulated Error against Black-Box Model polytropic index

This parameter was plotted for different values of the polytropic index as shown in Figure 10. An optimum value is established at $n = 1.51$. This gives the closest agreement between the analytical and Black-Box Model.

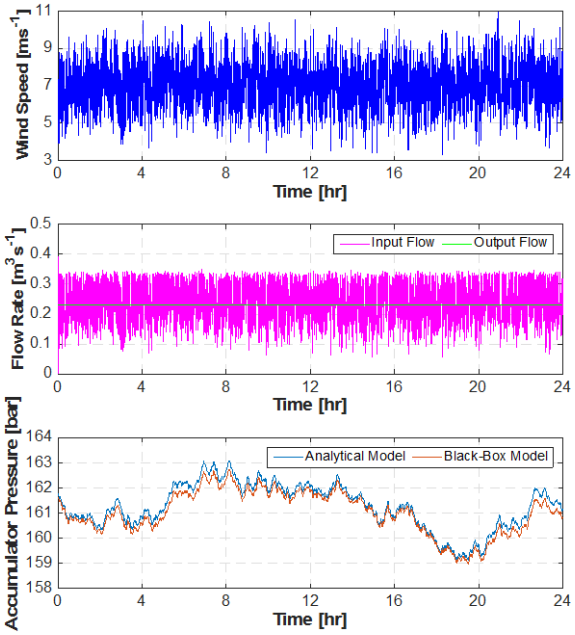

Figure 11: Wind Data and Pressure Response

The wind data and corresponding accumulator pressure response for both models are shown in

Figure 11. One can observe a very good agreement between the two. The motivation behind developing such a Black-Box Model for stochastic simulations is justified by computational demands. The computational time for the analytical model can be extremely long due to the very small time-steps required to adequately resolve the detailed thermodynamic response when using a realistic stochastic input. The computational times corresponding to the results shown in Figure 11 are shown in Table 5. Clearly there is a significant difference when using the Black-Box Model.

Table 5: Comparison of Computational Cost

Time-series Length	Analytical Model	Black-Box Model
24 hours	42.6 hours	4.7 seconds

Despite its much faster execution time, the Black-Box Model has a significant drawback. It is unable to account for heat transfer when the accumulator is at rest, that is, when it is not charging or discharging. This can lead to it over-estimating the operating efficiency of the system. In order to verify the extent of this drawback in the context of a stochastic simulation, the efficiencies were calculated for the simulation run in Figure 11. The energy efficiency for such a device can be defined as follows:

$$\eta = \frac{E_{adi}^{(n_s)} - E_{adi}^{(1)}}{W} \tag{11}$$

where W is the net work-done on the gas and $E_{adi}^{(1)}$, $E_{adi}^{(n_s)}$ represent the *adiabatically-stored* energy at the initial and final time steps respectively. The term adiabatically-stored energy refers to the work that would be done by that volume of gas if it were to be expanded adiabatically to atmospheric pressure [17], that is:

$$E_{adi} = V_{air}\left[p_{acc}\frac{(1 - v_r{}^{\gamma-1})}{\gamma - 1} - p_{atm}(v_r - 1)\right] \tag{12}$$

The term v_r represents a compression ratio: it is the ratio of the final expanded air volume (V_{tot}) to the current compressed volume (V_{air}). The work input can be computed using numerical integration:

$$W = \sum_{i=1}^{n_s-1}\left\{p_{acc}^{(i)}\left(V_{air}^{(i+1)} - V_{air}^{(i)}\right)\right\} \tag{13}$$

Based on the above definition it can be noted that work done on the gas is positive whereas work done by the gas is negative.

The principle behind the definition of efficiency in equation (11) is that over a period of operation, work is being done on the gas and by the gas. The net work done should correspond to a resulting change in the adiabatically-stored energy of the system. For perfect adiabatic operation the two terms would be equal, but due to thermal losses, the adiabatically-stored energy is lower.

Table 6: Operating Efficiencies for Stochastic Case

Analytical Model	Black-Box Model
96.88%	98.67%

The efficiencies computed from each model are shown in Table 6. As expected, the Black-Box Model over-predicts efficiency since it cannot account for thermal losses when no charging/discharging is taking place. However, the difference between the two is minimal. This indicates that during the 24 hour time-series there were very few cases in which the storage device was not being charged or discharged. It can therefore be verified that the Black-Box Model with a polytropic index of $n = 1.51$ is adequate for such stochastic simulation runs.

Although the efficiency seems very high, it must be noted that the value only represents the efficiency of the compression/expansion process, as hydraulic losses are not accounted for. Nonetheless, it is still relatively high and this results from the design of the system where the floating chamber dissipates the pressure fluctuations. Minimal pressure changes imply minimal temperature changes, and therefore the internal air condition does not deviate significantly from its initial steady-state temperature. This implies that there is limited heat-exchange with the surroundings. Loss of thermal energy to the surroundings is a key form of energy loss during a compression process, so mitigating this effect increases the efficiency.

5 CONCLUDING REMARKS

This work has modelled the performance of a hydro-pneumatic energy storage device operating in a central Mediterranean climate. It was shown that the pressure response of the device is dependent on the compression rate, as this affects the extent of the heat exchange with the surroundings. On the other hand, seasonality did not play a significant role. In fact, both the response and the efficiency were practically identical for the two extreme months. This is due to the thermal equilibrium that is established with the surroundings, and any fluctuations are relative to this condition. Such performance bodes well in terms of consistency.

A computationally efficient Black-Box Model was successfully correlated using a curve fitting process. The ideal value was established by considering the error between the response to a stochastic input using the analytical and simplified

model. A value of $n = 1.51$ yielded the lowest accumulated error. Finally, it can be observed that although the Black-Box Model cannot account for thermal losses when the system is not charging or discharging, the associated over-prediction is minimal. This implies that simulations with realistic stochastic inputs where the system operates continuously could make use of the more computationally efficient model.

Future work will continue to improve the understanding of the thermodynamic processes in such a device. A 1:10 prototype is presently being designed and will be deployed in Maltese waters in the near future. The aim is to measure its performance under real-time operational conditions and to identify practical and logistical challenges. The hydrodynamic characteristics are also within the scope of future work, particularly in open sea conditions. Finally, there is also interest to study the implications of a hollow floating platform on the deployment of TLPs, which presently offers a significant logistical hurdle.

ACKNOWLEDGEMENTS

Project *FLASC* (*R&I-2015-044-T*) is financed by the Malta Council for Science & Technology, for and on behalf of the Foundation for Science and Technology, through the FUSION: R&I Technology Development Programme. This research is also partly funded by the Malta Government Scholarship Scheme.

This research has been carried out using computational facilities procured through the European Regional Development Fund, Project ERDF-080 '*A Supercomputing Laboratory for the University of Malta*'.

The authors would also like to thank the Knowledge Transfer Office at the University of Malta.

The energy storage platform described in this paper is patent pending (PCT/IL2016/050100).

REFERENCES

[1] F. Steinke, P. Wolfrum, and C. Hoffmann, "Grid vs. storage in a 100% renewable Europe," *Renewable Energy*, vol. 50, pp. 826-832, February 2013.

[2] M. Y. Suberu, M. W. Mustafa, and N. Bashir, "Energy storage systems for renewable energy power sector integration and mitigation of intermittency," *Renewable and Sustainable Energy Reviews*, vol. 35, no. 7, pp. 499-514, July 2014.

[3] E. Hittinger, J. F. Whitacre, and J. Apt, "What properties of grid energy storage are most valuable?," *Journal of Power Sources*, vol. 206, no. 1, pp. 436-449, January 2012.

[4] S. D. Garvey et al., "On generation-integrated energy storage," *Energy Policy*, vol. 86, no. 11, pp. 544-551, November 2015, http://dx.doi.org/10.1016/j.enpol.2015.08.001.

[5] W. Musial and B. Ram, "Large-Scale Offshore Wind Power in the United States - Assessment of Opportunities and Barriers," NREL, NREL/TP-500-40745, 2010.

[6] A. H. Slocum, "Symbiotic Offshore Energy Harvesting and Storage Systems," *Sustainable Energy Technologies and Assessments*, vol. 11, no. 9, pp. 135-141, September 2015.

[7] D. Buhagiar, T. Sant, C. Micallef, and R. N. Farrugia, "Improving the Energy Yield from an Open Loop Hydraulic Offshore Turbine through Deep Sea Water Extraction and Alternative Control Schemes ," *Energy*, 2015, dx.doi.org/10.1016/j.energy.2015.03.001.

[8] T. Sant, D. Buhagiar, and R. N. Farrugia, "Offshore Floating Wind Turbine-driven Deep Sea Water Pumping for Combined Electrical Power and District Cooling," in *Journal of Physics: Conference Series - The Science of Making Torque from Wind*, vol. 524, Copenhagen, 2014.

[9] J. Van de Ven and P. Y. Li, "Liquid piston gas compression," *Applied Energy*, vol. 86, no. 10, pp. 2183-2191, October 2009.

[10] D. Matha, "Model Development and Loads Analysis of an Offshore Wind Turbine on a Tension Leg Platform, with a Comparison to Other Floating Turbine Concepts," National Renewable Energy Laboratory, Denver, CO, M.Sc. Thesis NREL/SR-500-45891, 2010.

[11] D. Buhagiar and T. Sant, "Modelling Of A Novel Floating Platform With An Integrated Hydraulic Accumulator For Offshore Energy Storage Applications," in *OSES: The Offshore Energy and Storage Symposium*, Valletta, 2016.

[12] Frank M. White, *Viscous Fluid Flow*.: McGraw-Hill, 1991.

[13] N. A. Kermani and M. Rokni, "Heat transfer analysis of liquid piston compressor for hydrogen applications," *International Journal of Hydrogen Energy*, February 2015, In Press, Corrected Proof.

[14] NODC. (2013, June) National Oceanographic Data Centre. [Online]. http://www.nodc.noaa.gov/OC5/WOA09/pr_woa09.html

[15] D. Buhagiar, T. Sant, and M. K. Bugeja, "Control of an Open-Loop Hydraulic Offshore Wind Turbine Using a Variable-

Area Orifice," in *ASME 2015 34th International Conference on Ocean, Offshore and Arctic Engineering*, St. John's, 2015, doi:10.1115/OMAE2015-41388.

[16] E. W. Lemmon, R. T. Jacobsen, and S. G. Penoncello, "Thermodynamic Properties of Air and Mixtures of Nitrogen, Argon and Oxygen From 60 to 2000 K at Pressures to 2000 MPa," American Institue of Physics, Technical Report 0047-2689/2000/29(3)/331/55, 2000.

[17] P. Y. Li, J. D. Van de Ven, and C. Sancken, "Open accumulator concept for compact fluid power energy storage," in *International Mechanical Engineering Congress and R&D Exposition*, Seattle, 2007.